The Interplay of Size and Surface Functionality on the Cellular Uptake of Sub-10 nm Gold Nanoparticles

Ying Jiang,[†,‡] Shuaidong Huo,[†,§,‡] Tsukasa Mizuhara,[†] Riddha Das,[†] Yi-Wei Lee,[†] Singyuk Hou,[†] Daniel F. Moyano,[†] Bradley Duncan,[†] Xing-Jie Liang,[§] and Vincent M. Rotello*[,†]

[†]Department of Chemistry, University of Massachusetts Amherst, 710 North Pleasant Street, Amherst, Massachusetts 01003, United States and [§]Key Laboratory for Biological Effects of Nanomaterials and Nanosafety, National Center for Nanoscience and Technology, Chinese Academy of Sciences (CAS), No.11, First North Road, Zhongguancun, Beijing 100190, China. [‡]Y. J. and S. H. contributed equally to this work.

ABSTRACT Correlation of the surface physicochemical properties of nanoparticles with their interactions with biosystems provides key foundational data for nanomedicine. We report here the systematic synthesis of 2, 4, and 6 nm core gold nanoparticles (AuNP) featuring neutral (zwitterionic), anionic, and cationic headgroups. The cellular internalization of these AuNPs was quantified, providing a parametric evaluation of charge and size effects. Contrasting behavior was observed with these systems: with zwitterionic and anionic particles, uptake *decreased* with increasing AuNP size, whereas with cationic particles, uptake *increased* with increasing particle size. Through mechanistic studies of the uptake process, we can attribute these opposing trends to a surface-dictated shift in uptake pathways. Zwitterionic NPs are primarily internalized through passive diffusion, while the internalization of cationic and anionic NPs is dominated by multiple endocytic pathways. Our study demonstrates that size and surface charge interact in an interrelated fashion to modulate nanoparticle uptake into cells, providing an engineering tool for designing nanomaterials for specific biological applications.

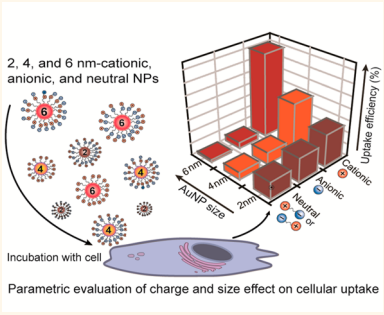

Parametric evaluation of charge and size effect on cellular uptake

KEYWORDS: endocytosis pathway · passive fusion · size-dependent · surface charge · sub-10 nm gold nanoparticles

The physicochemical properties of nanoparticles (NPs), in particular, size,[1−5] shape,[6−8] surface charge,[9−12] and functionality,[13−15] comprehensively determine the interactions of NPs with physiological systems.[16,17] Recent studies have generally attempted to correlate the NPs−cell interactions with the physical and structural properties of NPs on a case-by-case basis, looking at one parameter while keeping others constant. For example, the cellular uptake of nanoparticles was found to be strongly size-dependent, with 50 nm nanoparticles exhibiting the highest cellular uptake efficiency among a set of AuNP ranged in 10−100 nm.[7] In similar fashion, we and other groups have found that the internalization of NPs is dictated by chemical functionalities on nanoparticle surface.[9,15]

Exploring NP behavior in biological contexts along a single structural parametric axis is clearly informative. Interplay is expected, however, between structural factors, *e.g.*, size and surface properties in terms of the biological properties of nanomaterials. Examining the collective impact of these parameters in cellular internalization is crucial for generating effective tools for biomedical applications in delivery. For example, Chan *et al.* studied the roles of nanoparticle size (15, 30, 60, and 90 nm) and surface ligand grafting density on serum protein adsorption, showing how these attributes differentiated the pathway and efficiency of nanoparticle uptake by macrophage cells.[18] In another study, Toth *et al.* explored the effects of NP charge and size on the cellular uptake by changing the polymer coatings of AuNPs of 5, 10, and 20 nm sizes.[14]

Smaller (sub-10 nm) AuNP provide a particularly important set of particles for biomedical applications.[3,19−22] Pragmatically, these particles provide high payload-to-carrier ratios, with smaller particles in this regime capable of renal clearance.[23] On a fundamental level, these particles are on a size scale commensurate with proteins, and can be engineered to provide highly

* Address correspondence to rotello@chem.umass.edu.

Received for review June 10, 2015 and accepted October 4, 2015.

Published online October 05, 2015
10.1021/acsnano.5b03521

biomimetic surfaces.[24] Practically, however, the small size of these NPs makes parametric evaluation of surface chemistry challenging, as polymeric coatings will induce more dynamic changes in size and dynamic properties to smaller particles.

Here, we report the parametric fabrication of 2, 4, and 6 nm core AuNP featuring zwitterionic, anionic, and cationic surface ligands. We correlated the cellular internalization efficiency of these particles and observed a striking difference in uptake trends. With cationic particles, increasing particle size resulted in increasing uptake. The opposite trend was observed for neutral zwitterionic and anionic particles, where uptake efficiency decreased with particle diameter. Mechanistic studies provide insight into these opposing trends. With cationic particles, active endocytotic pathways were responsible for the bulk of NP uptake. With the zwitterionic particles, however, passive diffusion appeared to be the predominant mechanism. More interestingly, small sized anionic NP (2, and 4 nm) entered cells through endocytic pathways to that of same sized cationic particles, while large sized anionic particles (6 nm) mainly displayed caveolae/lipid raft-mediated pathway. The results reported here demonstrate the importance of the interplay between size and surface functionality on dictating nanoparticle–cell interactions, and offer insight into engineering NP systems with predictable cell interactions.

RESULTS AND DISCUSSION

Fabrication and Characterization of Sub-10 nm AuNPs. We designed structurally related NPs that featuring different surface charges to probe the effect of NP surface functionality on the cellular uptake of sub-10 nm AuNP. We first synthesized a set of cationic and anionic sub-10 nm AuNP coated with thioalkyl tetra(ethylene glycol)ated trimethylammonium (TTMA), and carboxylate ligands (COOH), respectively. The tetra(ethylene glycol) spacer was added between the terminal positively or negatively charged group and the hydrophobic alkyl chain to enhance NP stability, and to improve the biocompatibility of AuNP. The third category of sub-10 nm AuNP in this study was coated with zwitterionic ligands. We generated two subfamilies featuring different positioning of the charged moieties (Figure 1A), the first has positive charges in outermost

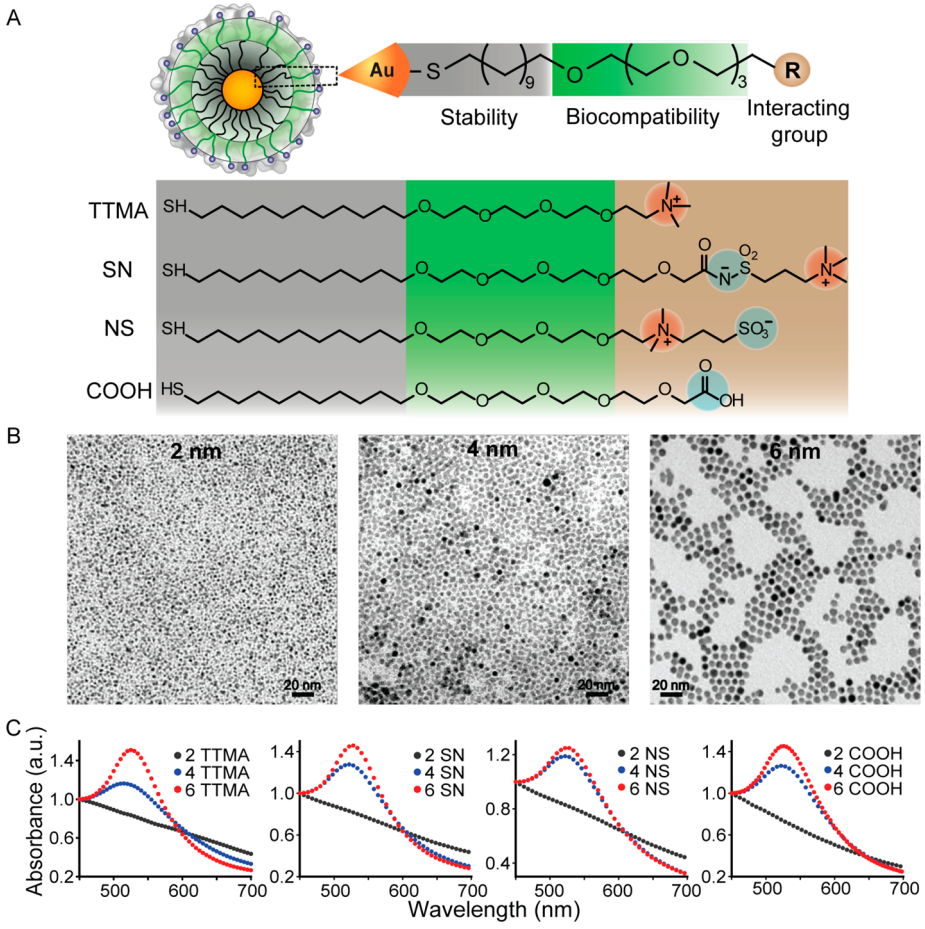

Figure 1. Characterization of as-synthesized gold nanoparticles with different sizes (2, 4, and 6 nm) and surface modification (cationic, TTMA; zwitterionic, SN and NS; and anionic, COOH). (A) General structure of AuNP, with either interactive cationic and anionic or "stealth" zwitterionic headgroups appended to a noninteracting OEG-functionalized interior. (B) TEM images of 2, 4, and 6 nm core diameter AuNPs. (C) UV–vis absorbance spectra of the each of the particle families as a function of core size.

TABLE 1. Dynamic Light Scattering Analysis and Zeta-Potential Measurements of As-Synthesized Nanoparticles in 5 mM Phosphate Buffer (pH = 7.4)

nanoparticles	hydrodynamic size (nm)	zeta-potential (mV)
2 TTMA	6.7 ± 0.4	18.2 ± 0.8
4 TTMA	8.6 ± 0.6	19.3 ± 0.3
6 TTMA	10.1 ± 1.1	17.5 ± 0.6
2 SN	6.7 ± 0.2	−3.6 ± 0.7
4 SN	8.9 ± 0.2	−4.8 ± 0.6
6 SN	12.5 ± 0.4	−6.1 ± 0.4
2 NS	6.1 ± 0.4	−3.7 ± 0.3
4 NS	7.7 ± 0.2	−7.9 ± 1.4
6 NS	10.6 ± 0.8	−10.0 ± 1.2
2 COOH	7.0 ± 0.2	−41.2 ± 1.7
4 COOH	8.2 ± 1.2	−42.8 ± 1.2
6 COOH	9.5 ± 1.3	−44.6 ± 1.5

layer (SN), while the second ligand has innermost layer of positive charge (NS).

The particles were fabricated using 2 nm NPs protected with 1-dodecanethiol synthesized according to the Brust method,[25] while 4 and 6 nm AuNP were grown from 2 nm dodecanethiol AuNP using heat-induced size evolution.[26] These AuNP were then functionalized with TTMA, COOH or zwitterionic ligands *via* place exchange reactions. The successful NP surface functionalization was analyzed and confirmed using laser desorption/ionization mass spectrometry (LDI-MS, Figure S1). A molecular peak observed at *m/z* value of 422.3 was ascribed to TTMA on NP surface, while peaks at 438.3, 530.2, and 601.1 were attributed to COOH, NS, and SN ligands, respectively. The number of ligands on each particle surface was determined by matrix-assisted laser desorption/ionization mass spectrometry (MALDI-MS, Table S1). The size and morphology of all NPs were further characterized using transmission electron microscopy (TEM) (Figure 1B) and dynamic light scattering (DLS) analysis. As shown in Table 1, the hydrodynamic size of AuNP increased gradually when the core size of NP was increased from 2 to 6 nm. Meanwhile, the functionalization of AuNP with TTMA, COOH, or zwitterionic surface ligands had minor effect on AuNP size. Zeta potential measurements confirmed the positive, negative, and neutral charges of TTMA, COOH, and zwitterionic ligand-coated AuNP, respectively (Table 1). As expected, UV spectra of AuNP indicated a red-shifted surface plasma resonance (SPR) peak when NP core size was increased from 2 to 6 nm, with no significant SPR band difference observed between the same size AuNP coated with TTMA, COOH, and zwitterionic ligands (Figure 1C).

Cellular Uptake of AuNPs. Our uptake studies used the widely employed human cervical carcinoma (HeLa) cell line, allowing the correlation of current study with prior reports. Preliminary studies indicated a low cytotoxicity of AuNP to HeLa cells at a NP concentration of 25 nM; this concentration was then fixed for the following NP

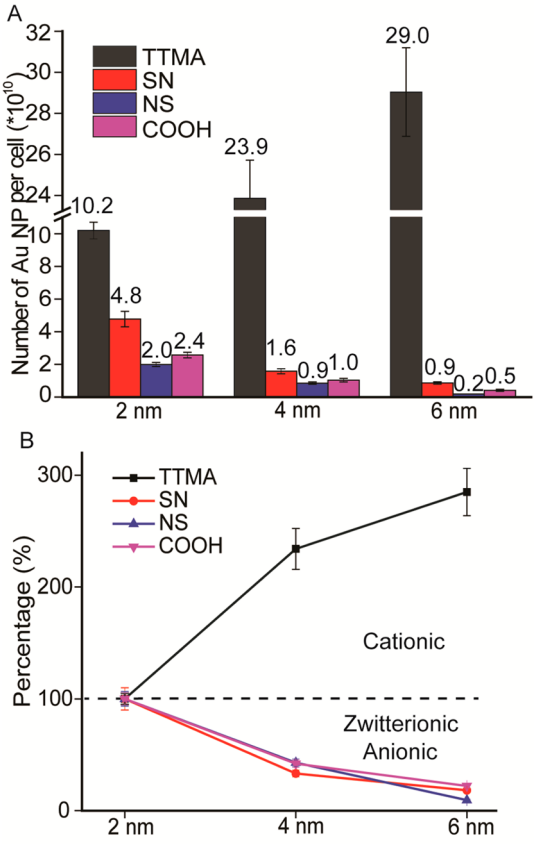

Figure 2. (A) Cellular uptake of as-synthesized gold nanoparticles with different size and varied surface charge by HeLa cells after 3 h incubation in serum-free media. The amount of gold per cell was determined by ICP-MS. Number of gold nanoparticles inside cells was also indicated above the histogram bar. (B) Size-dependent uptake trend of AuNP. The uptake efficiency of 4 and 6 nm NP was normalized to that of 2 nm NP featuring the same surface charge. Mean values ± standard deviation, *N* = 3.

uptake study (Figure S2). The cellular internalization of AuNP was studied by exposing NPs to HeLa cells, followed by extensive washing to remove NPs adsorbed to the cell surface. AuNP uptake was quantified using inductively coupled plasma mass spectrometry (ICP-MS), with the mass of intracellular gold converted to the AuNP number using a previously reported method.[7] As expected, all cationic AuNP featuring TTMA surface ligands enter cells in a significantly higher efficiency than that of neutral zwitterionic and anionic AuNP (Figure 2A). Interestingly, zwitterionic NPs with positive outmost layer charge (Au-SN) entered cells more efficiently than NPs with negative outmost layer charge (Au-NS), and anionic Au-COOH NPs, indicating the charge orientation of zwitterionic AuNP significantly affected NP internalization.

While there were no major surprises when looking at the functionality axis alone, parametric variation of charge and size generated unexpected interrelationships. For the cationic particles, increasing particle size from 2 to 6 nm increased uptake efficiency 3-fold (Figure 2B), a trend consistent with Chan's study of

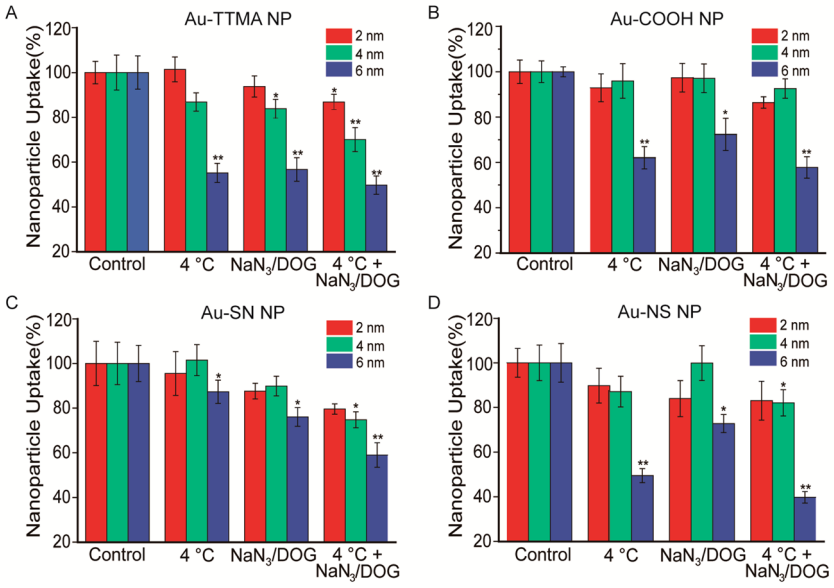

Figure 3. Uptake efficiency of (A) Au-TTMA NP, (B) Au-COOH NP, (C) Au-SN NP, and (D) Au-NS NP by HeLa cells in the absence or presence of sodium azide (NaN_3, 10 mM) and deoxy-glucose (DOG, 50 mM) at 4 or 37 °C after 3 h incubation in serum-free media. The cellular uptake efficiency of NPs (25 nM) was normalized to cells without inhibition treatment. Mean values ± standard deviation, $N = 3$. *$p < 0.05$, **$p < 0.01$ compared to each normalized control.

larger AuNPs.[18] A completely opposite trend was observed for both zwitterionic particles (NS and SN) and anionic particles, where increasing the core size decreased uptake, with 2 nm AuNPs uptaken >10-fold more efficiently than their 6 nm counterparts. This distinctive size dependence indicates that both particle size and surface functionality need to be considered together when designing carriers for cellular delivery.

Having found the size and surface charge dependence of the cellular uptake of AuNP in the absence of serum, we investigated further the uptake of these NP in complete cell culture medium containing 10% FBS, with the aim of understanding the effects of serum on NP uptake. For this purpose, HeLa cells were treated with NPs for 3 or 24 h in the presence of 10% FBS. The treatment of NPs (25 nM) had negligible cytotoxicity, with all treated cells having >90% viability 24 h post-treatment (Figure S3). The cellular uptake efficiency of different NP was similarly quantified using ICP-MS. As shown in Figure S4A, all NPs were internalized less efficiently in the presence of serum compared to that in serum-free medium after 3 h of treatment. Our results are similar to previous reports of multiple particles that showed decreased cellular uptake in the presence of serum, possibly due to the nonspecific binding of proteins to the cell membrane, a competitive process that slows the uptake of NPs when serum proteins are present.[7,27] Notably, similar size and charge-determined cellular uptake trends were still observed for both zwitterionic and anionic NPs in the presence and absence of serum, while cationic NPs exhibited a significantly different trend. With 4 nm, Au-TTMA NPs showed higher cellular uptake efficiency than that of 2 and 6 nm NPs in the presence of serum. In addition, the incubation of NPs with cells for 24 h showed similar size and charge-dependent cellular uptake, with enhanced number of NPs internalized to cells (Figure S4B). The different uptake trend of cationic NPs in the presence and absence of serum protein probably resulted from the distinct protein corona formation on the different sized particle surface, suggesting an indirect correlation between surface chemistry and biological response.[28]

Energy-Dependent Cellular Uptake Pathways of Sub-10 nm AuNPs. The opposite trends in size dependencies for neutral and charged particle uptake strongly suggested different mechanisms may be involved for the internalization of these NPs. Previous studies have shown that energy-dependent endocytosis is the predominant pathway for nanoparticle internalization, a process that can be suppressed through reduced temperature and ATP depletion.[29,30] Cooling cells to 4 °C only had minor effects on the uptake of any of the 2 nm particles (Figure 3, and Figure S5). For the cellular uptake of all NPs at reduced temperature, we observed strong size dependence. The 2 nm TTMA particles internalized much more efficiently than did the 6 nm TTMA NPs. With zwitterionic and anionic particles, little change of uptake was observed for the 2 and 4 nm NPs. The behavior of the 6 nm particles differed, however, with a modest decrease observed for the SN particle and a much larger decrease observed with the NS analogue and COOH particles. Qualitatively similar results were observed with pretreatment of cells with sodium azide (NaN_3, 10 mM)/2-deoxyglucose (DOG 50 mM) to deplete ATP, followed by AuNP exposure at 4 or 37 °C for ATP-depleted cells. Significantly, none

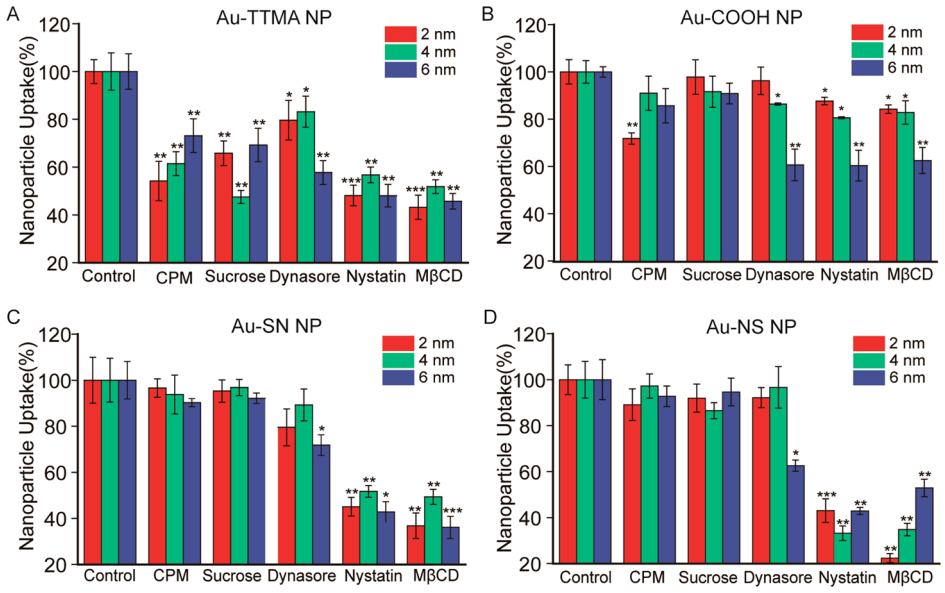

Figure 4. Uptake efficiency of (A) Au-TTMA NP, (B) Au-COOH NP, (C) Au-SN NP, and (D) Au-NS NP by HeLa cells in the presence of different endocytosis inhibitors. HeLa cells were treated with 25 nM NP for 3 h incubation in serum-free media. Mean values ± standard deviation, $N = 3$. *$p < 0.05$, **$p < 0.01$, ***$p < 0.001$ compared to each normalized control.

TABLE 2. Summary of Cellular Uptake Inhibition of NP in the Presence of Endocytic Inhibitors[a]

		2 nm				4 nm				6 nm			
inhibitors	**function**	**TTMA**	**SN**	**NS**	**COOH**	**TTMA**	**SN**	**NS**	**COOH**	**TTMA**	**SN**	**NS**	**COOH**
4 °C	Slow down metabolism	-	-	-	-	-	-	-	-	++	+	++	++
NaN_3 + DOG	ATP depletion	-	-	-	-	+	-	-	-	++	+	+	+
NaN_3 + DOG + 4 °C	ATP depletion/Slow down metabolism	+	-	-	-	++	+	+	-	++	++	++	++
Chlorpromazine (CPM)	Inhibits Rho GTPase (Clathrin)	++	-	-	++	++	-	-	-	++	-	-	-
Sucrose	Inhibits clathrin-mediated endocytosis	++	-	-	-	++	-	-	-	++	-	-	-
Dynasore	Inhibits Dynamin-GTPase	-	-	-	-	+	-	-	+	++	+	+	++
Nystatin	Inhibition of raft formation	+++	++	+++	+	++	++	++	+	++	+	++	++
MβCD	Cholesterol depletion/caveolae	+++	++	++	+	++	++	++	+	++	+++	++	++

[a] +, $p < 0.05$; ++, $p < 0.01$; +++, $p < 0.001$ through unpaired t-test between normalized control and inhibitor-treated groups. -: no significant inhibition.

of the 2 nm particles showed substantially different uptake under any of the conditions, strongly suggesting a different pathway was involved in the uptake of 2 nm NPs.

Endocytosis Inhibition of Sub-10 nm AuNPs. We next compared the effects of endocytosis inhibitors on NP uptake. We first studied the effects of chlorpromazine (CPM) and sucrose, which inhibit clathrin-mediated endocytosis.[31−35] As shown in Figure 4, CPM (28 nM) and sucrose (450 mM) pretreatments significantly inhibited the internalization of all TTMA-coated AuNPs. However, negligible inhibition effect was observed for zwitterionic and anionic AuNP with similar CPM and sucrose pretreatment, with no dependence on NP size, but with the exception that modest inhibition effect was observed for 2 nm Au-COOH NPs with CPM treatment.

We next pretreated cells with dynasore, an effective inhibitor of dynamin-dependent endocytosis.[36] We found that dynasore pretreatment significantly inhibited the internalization of all Au-TTMA NP and 6 nm zwitterionic AuNPs (Figure 4 and Table 2). A strong size dependence was also observed for anionic NPs; 2 nm Au-COOH particles were less inhibited by dynasore than the 6 nm NPs. These studies collectively show that TTMA particles and 2 nm Au-COOH particles are internalized through multiple endocytotic pathways, while dynamin-mediated endocytosis is the only operative endocytotic mechanism for zwitterionic and 6 nm anionic particles, a completely unexpected outcome.

Finally, we studied the uptake difference of AuNP in the presence of cholesterol depletion agents that inhibit lipid raft-mediated uptake, in particular both membrane fusion processes and caveolae-dependent endocytosis.[20,37−39] The pretreatment of cells with nystatin or methyl-β-cyclodextrin (MβCD) dramatically reduced uptake of all particles, including the 2 and 4 nm zwitterionic NPs that were unresponsive to other

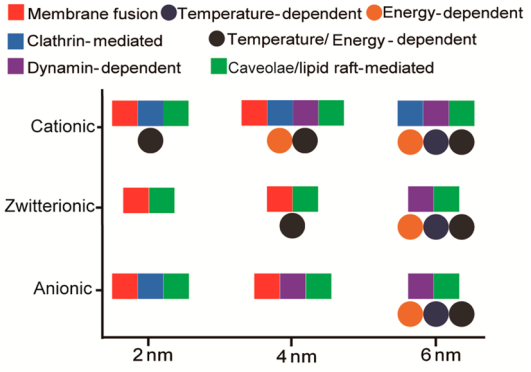

Scheme 1. Interplay of size and surface functionality on the cellular uptake pathway of AuNP.

inhibitors (Figure 4 and Table 2). To exclude the possibility that these inhibitors may have interfered with the uptake of particles by inducing toxicity to cells, we measured the viability of HeLa cells treated with inhibitors for 3 h, and did not find obvious toxicity (Figure S6).

Taken together, it is clear that the interplay of particle size and coverage plays a complex role in determining NP uptake. With cationic particles, multiple endocytic pathways, including clathrin- and caveolae/lipid raft-mediated endocytosis, were observed (Table 2 and Scheme 1). The zwitterionic NPs provided more specific mechanisms of uptake, with membrane fusion being the predominant mechanism for 2 and 4 nm zwitterionic NPs. In contrast, 6 nm zwitterionic NP were prone to enter cells through caveolae/lipid raft-mediated uptake, indicating a significant size-induced switching of the internalization mechanisms of NPs. Interestingly, 2 and 4 nm anionic particles displayed a similar multiple endocytic pathways to that of same sized cationic particles, while 6 nm anionic particles were internalized in caveolae/lipid raft-mediated pathway.

A key feature of our study is the importance of surface coverage in determining cell uptake efficiency and mechanism. The distinct energy-independent cellular uptake of 2 and 4 nm zwitterionic is consistent with the previous report by Alexander-Katz *et al.* that for small size NP (diameters $\leq$4 nm),[40] the monolayer contains a large amount of free volume that maximizes the ligand fluctuations and minimizes the energy barrier to "snorkeling", facilitating the energy-independent membrane fusion process for NPs to enter cells. The 6 nm zwitterionic and anionic NPs are above the size threshold for membrane fusion, so these NPs mainly enter cells *via* dynamin-dependent endocytosis pathway.

CONCLUSIONS

In summary, we have shown that there is a strong interrelationship between NP size and surface functionality on the cellular uptake of sub-10 nm gold nanoparticles. We have found that relatively small changes of NP core size were sufficient to induce dramatic changes in NP internalization efficiency and mechanism. These studies demonstrate that variation of particle size and coverage can be used synergistically to control cell uptake processes, an important design tool for bionanotechnology applications.

METHODS

Cell Culture. HeLa cells were purchased from American Type Culture Collection (ATCC, Manassas, VA) and maintained in low-glucose Dulbecco's modified Eagle's medium (DMEM) with 10% fetal bovine serum (FBS) and 1% antibiotic (100 U/mL penicillin and 100 μg/mL streptomycin). The cells were cultured at 37 °C under a humidified atmosphere of 5% CO_2.

Nanoparticle Uptake and Inhibition Studies. HeLa cells were seeded in a 48 well plate at a density of ~2 $\times$ 10^4 cells/well 24 h a day before experiment. At the day of incubation, cells were washed three time with phosphate buffered saline (PBS) and preincubated with the following endocytic inhibitors in serum free media for 1 h at 37 °C: methyl-β-cyclodextrin (10 mM), nystatin (180 nM), sodium azide (NaN_3, 10 mM) and 2-deoxyglucose (DOG, 50 mM), dynasore (80 μM), chlorpromazine hydrochloride (28 nM), and sucrose (450 mM). All inhibitors were purchased from Sigma except for dynasore which was obtained from Fisher Scientific, and the concentrations of the inhibitors were used according to previous reports.[15,30]

After 1 h, nanoparticles were added at a concentration of 25 nM and the mixtures were incubated for another 3 h at 37 °C in the presence of the inhibitors. Untreated cells were used as negative control, and cells treated with only NPs in the absence of inhibitors were used as positive control. After incubation, cells were washed five times with PBS buffer. Cell lysis buffer (250 μL per well) was used to lyse the cell, with the cell culture plate kept at room temperature on a vibrator for 30 min. In addition, a freeze/thaw cycle was also adopted to further facilitate the cell lysis process. After that, cells were digested with 0.5 mL of fresh *aqua regia* for 10 min. The digested samples were further processed for ICP-MS analysis to determine the intracellular amount of gold. Each cell uptake experiment was done in triplicate, and each replicate was measured 5 times by ICP-MS.

Temperature and Energy Dependent Pathways Study. HeLa cells were seeded in a 48 well plate at a density of 2 $\times$ 10^4 cells/well a day before experiment. At the day of incubation, cells were washed three times with PBS buffer and pretreated with 10 mM NaN_3 and 50 mM DOG at 4 °C for 1 h, then HeLa cell were incubated with 25 nM Au NPs in the presence of NaN_3/DOG at 4 °C for another 3 h.

Sample Preparation for ICP-MS and ICP-MS Measurements. For the quantitative determination of Au content in the cellular uptake study, the cell lysates were digested with 0.5 mL fresh *aqua regia* composed of hydrochloric acid and nitric acid (3:1, v/v) (highly corrosive and must be used with extreme caution!) for 10 min.[15,41,42] Then, each digested sample was diluted to 10 mL with deionized water. A series of gold standard solutions (20, 10, 5, 2, 1, 0.5, 0.2, and 0 ppb) were prepared at the same time. Each gold standard solution also contained 5% *aqua regia*. The gold standard solutions and cellular uptake sample solutions were measured on a PerkinElmer NexION 300X ICP mass spectrometer.

Particle uptake efficiency (%) was calculated based on the following equation:

$$\text{Uptake efficiency (\%)} = (\text{Number of NPs taken up by cells}/\text{Number of NPs incubated with cells}) \times 100\ \%$$

And inhibition efficiency (%) was calculated by the following equation: Inhibition (%) = (Number of NP uptake in the presence of inhibitors/Number of NP uptake in the absence of inhibitors) × 100%

Conflict of Interest: The authors declare no competing financial interest.

Acknowledgment. This work was supported by the grants from the NIH (EB014277), National Distinguished Young Scholars grant from NSFC (31225009) and financial support from China Scholarship Council. T.M. is grateful to the Japan Society for the Promotion of Sciences (JSPS) for a Postdoctoral Fellowship for Research Abroad.

Supporting Information Available: The Supporting Information is available free of charge on the ACS Publications website at DOI: 10.1021/acsnano.5b03521.

Nanoparticle synthesis and characterization, and additional experimental details and figures (PDF)

REFERENCES AND NOTES

1. Jiang, W.; Kim, B. Y. S.; Rutka, J. T.; Chan, W. C. W. Nanoparticle-Mediated Cellular Response is Size-Dependent. *Nat. Nanotechnol.* **2008**, *3*, 145–150.
2. Lundqvist, M.; Stigler, J.; Elia, G.; Lynch, I.; Cedervall, T.; Dawson, K. A. Nanoparticle Size and Surface Properties Determine the Protein Corona with Possible Implications for Biological Impacts. *Proc. Natl. Acad. Sci. U. S. A.* **2008**, *105*, 14265–14270.
3. Zhang, S. L.; Li, J.; Lykotrafitis, G.; Bao, G.; Suresh, S. Size-Dependent Endocytosis of Nanoparticles. *Adv. Mater.* **2009**, *21*, 419–424.
4. Huo, S. D.; Ma, H. L.; Huang, K. Y.; Liu, J.; Wei, T.; Jin, S. B.; Zhang, J. C.; He, S. T.; Liang, X. J. Superior Penetration and Retention Behavior of 50 nm Gold Nanoparticles in Tumors. *Cancer Res.* **2013**, *73*, 319–330.
5. Ma, X.; Wu, Y.; Jin, S.; Tian, Y.; Zhang, X.; Zhao, Y.; Yu, L.; Liang, X. J. Gold Nanoparticles Induce Autophagosome Accumulation through Size-Dependent Nanoparticle Uptake and Lysosome Impairment. *ACS Nano* **2011**, *5*, 8629–8639.
6. Yang, K.; Ma, Y. Q. Computer Simulation of the Translocation of Nanoparticles with Different Shapes across A Lipid Bilayer. *Nat. Nanotechnol.* **2010**, *5*, 579–583.
7. Chithrani, B. D.; Ghazani, A. A.; Chan, W. C. W. Determining the Size and Shape Dependence of Gold Nanoparticle Uptake into Mammalian Cells. *Nano Lett.* **2006**, *6*, 662–668.
8. Jin, S.; Ma, X.; Ma, H.; Zheng, K.; Liu, J.; Hou, S.; Meng, J.; Wang, P. C.; Wu, X.; Liang, X. J. Surface Chemistry-Mediated Penetration and Gold Nanorod Thermotherapy in Multicellular Tumor Spheroids. *Nanoscale* **2013**, *5*, 143–146.
9. Han, H. S.; Martin, J. D.; Lee, J.; Harris, D. K.; Fukumura, D.; Jain, R. K.; Bawendi, M. Spatial Charge Configuration Regulates Nanoparticle Transport and Binding Behavior. *Angew. Chem., Int. Ed.* **2013**, *52*, 1414–1419.
10. Cho, E. C.; Xie, J. W.; Wurm, P. A.; Xia, Y. N. Understanding the Role of Surface Charges in Cellular Adsorption *versus* Internalization by Selectively Removing Gold Nanoparticles on the Cell Surface with A I-2/KI Etchant. *Nano Lett.* **2009**, *9*, 1080–1084.
11. Verma, A.; Stellacci, F. Effect of Surface Properties on Nanoparticle-Cell Interactions. *Small* **2010**, *6*, 12–21.
12. Arvizo, R. R.; Rana, S.; Miranda, O. R.; Bhattacharya, R.; Rotello, V. M.; Mukherjee, P. Mechanism of Anti-Angiogenic Property of Gold Nanoparticles: Role of Nanoparticle Size and Surface Charge. *Nanomedicine* **2011**, *7*, 580–587.
13. Kostarelos, K.; Lacerda, L.; Pastorin, G.; Wu, W.; Wieckowski, S.; Luangsivilay, J.; Godefroy, S.; Pantarotto, D.; Briand, J. P.; Muller, S.; et al. Cellular Uptake of Functionalized Carbon Nanotubes is Independent of Functional Group and Cell Type. *Nat. Nanotechnol.* **2007**, *2*, 108–113.
14. Liang, M.; Lin, I. C.; Whittaker, M. R.; Minchin, R. F.; Monteiro, M. J.; Toth, I. Cellular Uptake of Densely Packed Polymer Coatings on Gold Nanoparticles. *ACS Nano* **2010**, *4*, 403–413.
15. Saha, K.; Kim, S. T.; Yan, B.; Miranda, O. R.; Alfonso, F. S.; Shlosman, D.; Rotello, V. M. Surface Functionality of Nanoparticles Determines Cellular Uptake Mechanisms in Mammalian Cells. *Small* **2013**, *9*, 300–305.
16. Albanese, A.; Tang, P. S.; Chan, W. C. W. The Effect of Nanoparticle Size, Shape, and Surface Chemistry on Biological Systems. *Annu. Rev. Biomed. Eng.* **2012**, *14*, 1–16.
17. Saha, K.; Bajaj, A.; Duncan, B.; Rotello, V. M. Beauty is Skin Deep: A Surface Monolayer Perspective on Nanoparticle Interactions with Cells and Biomacromolecules. *Small* **2011**, *7*, 1903–1918.
18. Walkey, C. D.; Olsen, J. B.; Guo, H. B.; Emili, A.; Chan, W. C. W. Nanoparticle Size and Surface Chemistry Determine Serum Protein Adsorption and Macrophage Uptake. *J. Am. Chem. Soc.* **2012**, *134*, 2139–2147.
19. Khlebtsov, N.; Dykman, L. Biodistribution and Toxicity of Engineered Gold Nanoparticles: A Review of *in Vitro* and *in Vivo* Studies. *Chem. Soc. Rev.* **2011**, *40*, 1647–1671.
20. Jiang, Y.; Tang, R.; Duncan, B.; Jiang, Z.; Yan, B.; Mout, R.; Rotello, V. M. Direct Cytosolic Delivery of siRNA Using Nanoparticle-Stabilized Nanocapsules. *Angew. Chem., Int. Ed.* **2015**, *54*, 506–510.
21. Huo, S. D.; Jin, S. B.; Ma, X. W.; Xue, X. D.; Yang, K. N.; Kumar, A.; Wang, P. C.; Zhang, J. C.; Hu, Z. B.; Liang, X. J. Ultrasmall Gold Nanoparticles as Carriers for Nucleus-Based Gene Therapy Due to Size-Dependent Nuclear Entry. *ACS Nano* **2014**, *8*, 5852–5862.
22. Huang, K. Y.; Ma, H. L.; Liu, J.; Huo, S. D.; Kumar, A.; Wei, T.; Zhang, X.; Jin, S. B.; Gan, Y. L.; Wang, P. C.; et al. Size-Dependent Localization and Penetration of Ultrasmall Gold Nanoparticles in Cancer Cells, Multicellular Spheroids, and Tumors *in Vivo*. *ACS Nano* **2012**, *6*, 4483–4493.
23. Zhou, C.; Long, M.; Qin, Y. P.; Sun, X. K.; Zheng, J. Luminescent Gold Nanoparticles with Efficient Renal Clearance. *Angew. Chem., Int. Ed.* **2011**, *50*, 3168–3172.
24. De, M.; You, C. C.; Srivastava, S.; Rotello, V. M. Biomimetic Interactions of Proteins with Functionalized Nanoparticles: A Thermodynamic Study. *J. Am. Chem. Soc.* **2007**, *129*, 10747–10753.
25. Brust, M.; Walker, M.; Bethell, D.; Schiffrin, D. J.; Whyman, R. Synthesis of Thiol-Derivatised Gold Nanoparticles in A Two-Phase Liquid-Liquid System. *J. Chem. Soc., Chem. Commun.* **1994**, 801–802.
26. Teranishi, T.; Hasegawa, S.; Shimizu, T.; Miyake, M. Heat-Induced Size Evolution of Gold Nanoparticles in the Solid State. *Adv. Mater.* **2001**, *13*, 1699–1701.
27. Kim, C. S.; Le, N. D.; Xing, Y.; Yan, B.; Tonga, G. Y.; Kim, C.; Vachet, R. W.; Rotello, V. M. The Role of Surface Functionality in Nanoparticle Exocytosis. *Adv. Healthcare Mater.* **2014**, *3*, 1200–1202.
28. Monopoli, M. P.; Aberg, C.; Salvati, A.; Dawson, K. A. Biomolecular Coronas Provide the Biological Identity of Nanosized Materials. *Nat. Nanotechnol.* **2012**, *7*, 779–86.
29. Kim, J. S.; Yoon, T. J.; Yu, K. N.; Noh, M. S.; Woo, M.; Kim, B. G.; Lee, K. H.; Sohn, B. H.; Park, S. B.; Lee, J. K.; Cho, M. H. Cellular Uptake of Magnetic Nanoparticle is Mediated through Energy-Dependent Endocytosis in A549 Cells. *J. Vet. Sci.* **2006**, *7*, 321–326.
30. Wang, L. M.; Liu, Y.; Li, W.; Jiang, X. M.; Ji, Y. L.; Wu, X. C.; Xu, L. G.; Qiu, Y.; Zhao, K.; Wei, T. T.; et al. Selective Targeting of Gold Nanorods at the Mitochondria of Cancer Cells: Implications for Cancer Therapy. *Nano Lett.* **2011**, *11*, 772–780.
31. McMahon, H. T.; Boucrot, E. Molecular Mechanism and Physiological Functions of Clathrin-Mediated Endocytosis. *Nat. Rev. Mol. Cell Biol.* **2011**, *12*, 517–533.
32. Stuart, A. D.; Brown, T. D. K. Entry of Feline Calicivirus is Dependent on Clathrin-Mediated Endocytosis and Acidification in Endosomes. *J. Virol.* **2006**, *80*, 7500–7509.
33. Liu, Y.; Kim, Y. J.; Ji, M.; Fang, J.; Siriwon, N.; Zhang, L. I.; Wang, P. Enhancing Gene Delivery of Adeno-Associated Viruses by Cell-Permeable Peptides. *Mol. Ther.-Methods Clin. Dev.* **2014**, *1*, 12.

34. Madani, F.; Lindberg, S.; Langel, U.; Futaki, S.; Gräslund, A. Mechanisms of Cellular Uptake of Cell-Penetrating Peptides. *J. Biophys.* **2011**, *2011*, 1–10.
35. Zhu, J.; Liao, L.; Zhu, L. N.; Zhang, P.; Guo, K.; Kong, J. L.; Ji, C.; Liu, B. H. Size-Dependent Cellular Uptake Efficiency, Mechanism, and Cytotoxicity of Silica Nanoparticles toward HeLa Cells. *Talanta* **2013**, *107*, 408–415.
36. Macia, E.; Ehrlich, M.; Massol, R.; Boucrot, E.; Brunner, C.; Kirchhausen, T.; Dynasore, A. Cell-Permeable Inhibitor of Dynamin. *Dev. Cell* **2006**, *10*, 839–850.
37. Nabi, I. R.; Le, P. U. Caveolae/raft-Dependent Endocytosis. *J. Cell Biol.* **2003**, *161*, 673–677.
38. Rodal, S. K.; Skretting, G.; Garred, O.; Vilhardt, F.; Van Deurs, B.; Sandvig, K. Extraction of Cholesterol with Methyl-b-cyclodextrin Perturbs Formation of Clathrin-Coated Endocytic Vesicles. *Mol. Biol. Cell* **1999**, *10*, 961–974.
39. Verma, A.; Uzun, O.; Hu, Y. H.; Hu, Y.; Han, H. S.; Watson, N.; Chen, S. L.; Irvine, D. J.; Stellacci, F. Surface-Structure-Regulated Cell-Membrane Penetration by Monolayer-Protected Nanoparticles. *Nat. Mater.* **2013**, *12*, 376–376.
40. Van Lehn, R. C.; Atukorale, P. U.; Carney, R. P.; Yang, Y. S.; Stellacci, F.; Irvine, D. J.; Alexander-Katz, A. Effect of Particle Diameter and Surface Composition on the Spontaneous Fusion of Monolayer-Protected Gold Nanoparticles with Lipid Bilayers. *Nano Lett.* **2013**, *13*, 4060–4067.
41. Zhu, Z. J.; Yeh, Y. C.; Tang, R.; Yan, B.; Tamayo, J.; Vachet, R. W.; Rotello, V. M. Stability of Quantum Dots in Live Cells. *Nat. Chem.* **2011**, *3*, 963–968.
42. Liu, X.; Atwater, M.; Wang, J.; Huo, Q. Extinction Coefficient of Gold Nanoparticles with Different Sizes and Different Capping Ligands. *Colloids Surf., B* **2007**, *58*, 3–7.